Hair cell population integrity necessary to preserve vestibular function

Louise Schenberg[1*], François Simon[1,2*], *Aïda Palou*[3,4,5], *Cassandre Djian*[1], *Michele Tagliabue*[1], *Jordi Llorens* [2,3,4], *Mathieu Beraneck* [1]

1- Université Paris Cité, CNRS UMR 8002, INCC - Integrative Neuroscience and Cognition Center, F-75006, Paris, France.

2- Department of paediatric otolaryngology, Hôpital Necker-Enfants Malades, APHP, F-75015, Paris, France.

3- Departament de Ciències Fisiològiques, Universitat de Barcelona, 08907 l'Hospitalet de Llobregat, Catalunya, Spain.

4- Institut de Neurociènces, Universitat de Barcelona, Barcelona, Catalunya, Spain.

5- Institut d'Investigació Biomèdica de Bellvitge (IDIBELL), 08907 l'Hospitalet de Llobregat, Catalunya, Spain.

* These two authors contributed equally to this work.

Corresponding authors:

Pr Jordi Llorens, Universitat de Barcelona, 08907 l'Hospitalet de Llobrega, Catalunya, Spain. E-mail : jllorens@ub.edu

Dr. M. Beraneck. CNRS UMR 8002, Université Paris Cité, 45 rue des St-Pères, Paris 75270, France. Email: mathieu.beraneck@cnrs.fr

Funding: This work is supported by the Centre National d'Etudes Spatiales, the Centre National de la Recherche Scientifique, and the Université Paris Cité. MB and LS received funding from the Agence Nationale de la Recherche (ANR-20-CE37-0016 INVEST; ANR-22-CE37-002 LOCOGATE). CD received a research fellowship from the société Française d'ORL. MB & FS received funding from the ERANET NEURON Program VELOSO (ANR-20-NEUR-0005). AP & JL received funding from the ERANET NEURON Program VELOSO (grant PCI2020-120681-2 from MCIN/ AEI/10.13039/501100011033 and NextGenerationEU/PRTR).

Acknowledgment: this study contributes to the IdEx Université de Paris ANR-18-IDEX-0001. This work has benefited from the support and expertise of the animal facility of BioMedTech Facilities at Université Paris Cité ((https://biomedicale.u-paris.fr/biomedtech-facilities/)

INSERM US36 | CNRS UAR2009 | Université Paris Cité). The confocal microscopy studies were performed at the Centres Científics i Tecnològics de la Universitat de Barcelona (CCiTUB). We thank Dr. Benjamin Torrejon for technical assistance and Dr. Alberto Maroto for preliminary work for this study.

Author contribution: Conceptualization: JL ; MB. Methodology: LS ; AP ; FS ; MT ; JL ; MB. Formal analysis: LS ; AP ; CD; MT ; JL ; MB. Investigation: LS ; AP ; CD ; MB . Writing original manuscript: LS ; MB. Writing review and editing: LS ; ; FS ; MT ; JL ; MB. Visualization: LS ; AP ; MT ; JL ; MB. Supervision: LS ; FS; MT ; JL ; MB. Project administration: JL; MB. Funding acquisition: JL; MB.

Declaration of interests: The authors declare no competing interests.

SUMMARY

Regeneration of hair cells is a primary target of gene therapy aimed at restoring vestibular and cochlear functions[1]. Indeed, vestibular dysfunction constitutes a major medical concern, as one of its manifestation, dizziness, affects 15–35% of the general population, with a prevalence rate of 85% for those over 80 of age [2,3]. Age-related alterations of both vestibular function[4] and the integrity of vestibular hair cells has been reported in humans[5–8]. However, direct comparisons between structural pathology and vestibular dysfunctions quantifications are lacking in humans and rather limited in animal models[4,9], representing a significant gap in current knowledge.

Thus far, therapeutic trials in animal models targeting vestibular loss associated with genetic diseases have yielded varied and partial results[1,10–12], and the functional identity and quantity of hair cells sufficient to restore minimal or normal vestibular function remain undefined. Here, we further develop an innovative methodology[9] to bridge the gap between hair cells integrity and functional vestibular loss in individuals. Gradual vestibular deficits were induced through a dose-dependent ototoxic compound, quantified with canal or utricular-specific vestibulo-ocular reflex tests, and were then correlated in all individuals with the loss of type I and type II hair cells in different regions of ampulla and macula. Our findings reveal that the structure-function relationship is nonlinear, with lower bound of approximately 50% of hair cells necessary to retain minimal vestibular function, and threshold exceeding 80% to preserve normal function, thus shedding light on population-coding mechanisms for vestibular response. Our data further support[13] the decisive role of type I, rather than type II, HC in the tested VOR functions.

RESULTS

Dose-dependent effects of the treatment on the canal- and otolith-dependent VOR.

To investigate the dose-response effect of the ototoxic substance 3,3’-iminodiproprionitrile (IDPN), we performed in adult C57Bl6/J mice a single IP injection of IDPN at increasing doses: 0 (Control, n=7), 16 (n=8), 24 (n=8), 32 (n=7) and 40 (n=6) mmol/kg. Organ-specific vestibular function was quantified using gaze stabilizing reflexes tests before the injection, then 2 and 3

weeks after. There was no significant difference between vestibular function observed at D14 and D21 (mixed model analysis, see Supplementary Figure 1), confirming that the IDPN-induced toxicity is stable after 2 weeks[14,15] .To reduce measurement noise, data from D14 and D21 are pooled in the rest of the manuscript.

Horizontal canal function was assessed with two complementary tests. First, horizontal sinusoidal rotations at different frequencies were performed in the dark to record the angular horizontal vestibulo-ocular reflex (aVOR) the gain of which are shown in the bode plots of Figure 1.A for the different groups and tested frequencies. IDPN exposure at different doses (abbreviated as [X]mmol/kg) leads to a significant decrease of the aVOR gain for concentrations above [16] (Interaction Dose x Frequencies $F(16, 124)=15.4$, $p<0.0001$, see statistics table 1). The aVOR gain of the [24] group is decreased by ~50% compared to the Control group ([Control] vs [24]; at 0.2Hz, $p=0.0625$; 0.5Hz, $p=0.0147$; 0.8Hz, $p=0.0351$; 1Hz $p= 0.0454$ and 2Hz $p=0.0261$) and is significantly reduced by >90% at all frequencies for the 2 highest doses of [32] and [40] ($p<0.001$). The second test, Hsteps, consisting in a single abrupt horizontal acceleration (peak acceleration 500°/s²; Figure 1.B) shows a significant decrease of gain similar to aVOR for the 3 highest doses ($F(4, 31)=28.58$, $p<0.0001$; [Control] vs [16] $p=0.9956$; [Control] vs [24], [Control] vs [32] and [Control] vs [40], $p<0.001$). While the [32] and [40] groups have no residual response, the [24] group show an intermediate VOR loss ([16] vs [24] $p<0.001$; [24] vs [32] $p=0.0485$).

Specific otolithic (utricular) function was quantified using both static ocular counter-roll (OCR) measured during static head tilts, and dynamic OCR quantified during off-vertical axis rotation (i.e vertical component of eye movement during off-vertical axis rotation, see [16]). Similarly to its effect on canal function, IDPN leads to a significant decrease of both the static OCR (Figure 1.C) and dynamic OCR (Figure 1.D) gain for the 3 highest doses (static OCR $F(4, 31)=32.15$ $p<0.0001$, [Control] vs [24], [Control] vs [32] and [Control] vs [40] $p<0.001$; Dyn OCR $F(4, 31)=30.3$ $p<0.0001$, [Control] vs [24], [Control] vs [32], and [Control] vs [40] $p<0.001$), and an intermediate loss for the [24] group (static OCR [16] vs [24], $p=0.0021$; [24] vs [32], $p=0.023$; Dyn OCR [16] vs [24], $p<0.001$; [24] vs [32], $p=0.128$).

Taken together, these results reveal the dose-dependent effect of IDPN on the canal- and otolith-specific VORs in mice.

Dose-dependent effects of the treatment on the vestibular hair cells

105 To quantify the effect of the IDPN treatment on the vestibular HC, the vestibular organs were
106 removed and fixed in paraformaldehyde (4%) after VOR measurements at D21.
107 Immunochemistry was used to identify type I and type II HC with type-specific markers
108 (respectively osteopontin (SPP1) and calretinin (Calre)[17]). The total number of HC,
109 independently of their identity, was quantified using the pan-hair cell marker Myo7a. Figure
110 2.A shows typical examples of confocal (Zeiss LSM 880) immunostaining data obtained from
111 [Control], [24] and [40] groups.
112 The results of HC quantification are plotted in Figure 2.B, C and D, respectively for Myo7a (all
113 HC), SPP1 (type I-specific) and Calre (type II-specific) for both central and peripheral part of
114 the horizontal crista (see Supplementary Figure 2 for otolith cell counting). IDPN exposure
115 leads to a significant decrease in the number of Myo7a-labelled HC in the central part for all
116 doses and in the peripheral region for doses above [16] (see Figure 2.B). The [24] treatment
117 reduces by ~50% Myo7a+ labelled cells compared to the Control group (Central: [Control] vs
118 [24], $p<0.0001$; Peripheral: [Control] vs [24], $p<0.0001$). The two highest doses, though not
119 different from each other (Central: [32] vs [40] and Peripheral: [32] vs [40] $p>0.99$), lead to a
120 further 25% decrease in the number of Myo7a+ cells compared to the [24] group (Central:
121 [24] vs [40] $p=0.002$; Peripheral: [24] vs [40] $p<0.0001$).
122 The decrease in the number of vestibular type I HC labelled by SPP1 is shown in Figure 2.C
123 with a similar trend than the Myo7a labelling: loss is significant for all doses > [16] in the
124 central and the peripheral regions (Central: [Control] vs [24] and Peripheral: [control] vs [24],
125 $p<0.0001$). In contrast, IDPN did not lead to any change in the number of type II HC (Calre
126 labelled cells) in the central part of the crista, and to a small and non-significant decrease
127 limited to the highest dose of 40mmol/kg in the peripheral region (Central: [Control] vs [40]
128 $p>0.99$; Peripheral: [Control] vs [40] $p=0.8066$).
129 To determine how the HC loss compares in both organs for all individuals, we compared Type
130 I and Type II HC in all regions (Figure 2.E, top panel) by plotting a heat map based on the
131 Pearson correlation matrix (Figure 2.E, bottom panel). While the correlation between type I
132 HC remaining after IDPN is high in all regions, the correlation of Type II HC with type I HC is
133 low. Figure 2.F, 2.G and 2.H illustrate the different sorts of correlation found between the HC
134 identity and regions. The high correlation between the remaining Type I HC in the otolith and
135 canal organs (Central: $r^2=0.849$, $p<0.001$; Figure 2.F) shows that the IDPN treatment leads to
136 a highly correlated loss in both structures for all doses. However, there is no correlation

between the loss of Type I and Type II HC in the central regions of either organ (Canal: r^2=0.017, p=0.456; Figure 2.G) and a small yet significant correlation in the peripheral regions (Otolithic r^2=0.29, p<0.001; Figure 2.H) mostly driven by the small decrease in type II HC at the highest dose. This analysis also shows that the ototoxicity similarly affects canals and otoliths. Overall, the effect of the IDPN treatment leads to a largely specific dose-dependent loss of type I HC, with a comparable effect in central and peripheral regions of the ampulla and utricule.

Organ-specific structure-function relationship.

To investigate the relation between type I HC population of the different organs and the related vestibular function, we first compared the normalized individual gains of the vestibulo-ocular reflexes and the normalized number of type I (SPP1-labelled cells) HC in the central region of the canals (Figure 3.A and 3.B) and otoliths (Figure 3.C and 3.D). Normalization values were obtained using the mean of the control group (yellow dots) as maximal function (100%).

The relationship between the number of type I HC and the vestibular functions was approximated by interpolating the data with 2D sigmoidal curves accounting for both the vertical (measured function values) and horizontal (HC staining data) variability. Figure 3.A-D (canals, Figure 3.A and B; otoliths Figure 3.C and D) shows that the non-linearity of the HC-function relationship is particularly evident for canal tests. Figure 3.E-H illustrate the absence of correlation between the gains measured and the number of type II HC counted in the central regions of both vestibular organs (canals, Figure 3.E-F; otoliths Figure 3.G-H).

Since IDPN treatment differentially affects specific regions and cell types (Figure 2), we calculated the different Fit Error (%) of the sigmoids to determine which region/cell type better relates to the various VOR tests. This parameter is plotted for each test, and for the central and peripheral regions of each organ, considering either type I (SPP1 marker), type II (Calre marker) or both HC (type I + type II) (aVOR, Figure 3.I; HSteps Figure 3.J; OCR Figure 3.K; Dyn OCR Figure 3.L). In all instances, models based on type I HC always better approximate the function than models based on type II HC (i.e make less error; compare blue and yellow plots). Models based on type II HC in the periphery perform better than models based on type II HC in central parts, which probably relates to the partial and small dose-dependent effect found for the highest concentrations of IDPN (e.g. Fig 2.D, G, H). Finally,

169 using a model summing central and peripheral type I and type II HC led to a similar (3.I-K) or
170 smaller (3.L) error and thus better represented all the different VOR tests (compare dark and
171 colored plots in panels 3.I-L).
172 Overall, these results demonstrate that the responses to these different VOR tests strongly
173 depend on the integrity and proportion of type I HC. In the instances where all type I HC are
174 lost, the presence of type II HC alone does not allow to preserve the function. These targeted
175 analyses also suggested that the different VOR tests have differential dependency on the
176 amount of HC preserved. We therefore decided to investigate which quantity of total HC is
177 necessary for the maintenance of minimal or normal VOR function.
178
179 **Thresholds of minimal and normal population-coding in canal and otolith functions**
180 To determine these thresholds, we first grouped the mice based on their loss of type I HC
181 observed in the different organs. As shown in Figure 4.A, there is a large intra-group variability
182 and inter-group overlap in the amount of HCI left in all regions, leading to an apparent
183 continuum of type I HC integrity that ranges from the control animals (yellow) to the highest
184 dose of the treatment ([40], dark purple). However, a cluster analysis on this dataset revealed
185 3 distinct categories of animals characterized by high (green), intermediate (orange), or low
186 (pink) type I HC population integrity (Figure 4.B). We then validated that Myo7a is a pan-hair
187 cell marker which in both canals (Figure 4.C) and otoliths (Figure 4.D) closely matches the
188 number of both type I and type II HC. The high correlation between the addition of type I +
189 type II and myo7a-labelled cells (Canals $r^2=0.99$, $p<0.0001$ Figure 4.C; Otoliths $r^2=0.979$,
190 $p<0.0001$, Figure 4.D) is maintained for all 3 clusters, demonstrating that despite the ototoxic
191 alteration of the HC, this marker remains an accurate index of total HC integrity in all our
192 experimental conditions.
193 In Figure 4.E-H, a comprehensive analysis of the global structure-function relationship
194 encompassing all the hair cells was conducted by applying to the total hair cell (HC) residual
195 number the same sigmoidal fitting procedure employed for the specific HC types and
196 locations (Figure 3). For each test, we defined the minimal function thresholds as the
197 "*mean+SD*" gain of the low response cluster (pink dotted lines), while the normal vestibular
198 function threshold was defined as the "*mean-SD*" gain of the high response cluster (green
199 dotted lines). Using this methodology, normal thresholds represented >80% of function, while

200 minimal threshold represents < 20% of function (ordinate of the horizontal dotted line on
201 panels 4E-H).
202 The corresponding HC thresholds were then measured as the intercept between the function
203 thresholds and the sigmoid curve. The quantity of HC to preserve minimal horizontal canal
204 function was calculated at 57.8% for aVOR (Figure 4.E) and 57.03% for Hsteps (Figure 4.F),
205 while the threshold for normal functions were calculated at 65.9% and 62.5%, respectively.
206 Minimal HC thresholds for otolithic-dependent responses were slightly higher with lower
207 bounds calculated at 63.5% and 60.9% respectively for static OCR (Figure 4.G) and Dynamic
208 OCR (Figure 4.H). The HC thresholds for normal otolithic function were calculated at 73.1%
209 and 78.5%, respectively, slightly higher than for canal function. This analysis suggests that
210 canal-dependent function tested in our protocol remains in normal range when roughly 2/3
211 of HC are preserved, but requires about 1/2 of HC to preserve minimal function. On the other
212 hand, otolith-dependent function tested in our protocol requires approximatively 2/3 of HC
213 to maintain minimal function and ¾ of HC to remain in normal range,
214 To further highlight the relation between the total number of hair cells in ampulla and macula
215 and organ-specific function, the non-linear fits of the normalized vestibular function
216 presented in panels 4E-H are superimposed on Figure 4I. This summary scheme illustrates
217 that despite the experimental variability in measurements, inter-individual variability, and
218 differences in the parameters tested (static vs dynamic; long-lasting vs instantaneous
219 responses), all vestibulo-ocular reflexes show a rather comparable dependency on the HC
220 population integrity necessary to drive the eye movements, with no response observed when
221 50% of hair cell are lost, intermediate response when HC population is in range 50-80%, and
222 normal function for both organs when HC integrity is >80%.
223

224 **DISCUSSION**

225

226 In this study, we examined the effects of acute injections of increasing doses of an ototoxic
227 compound (3,3'-Iminodipropionitrile) on vestibular hair cell loss. Our findings align with
228 previous studies[14,15,18,19], confirming that IDPN induces dose-dependent, graded vestibular HC
229 loss, demonstrated through the use of the pan-hair cell marker Myo7a and the type I-specific
230 marker SPP1. However, our results further the understanding of vestibular loss of function by

correlating the remaining hair cells with the vestibular function at the individual and population level with organ-specific tests (canal or otolithic) and hair cells quantification. Our results clearly show that IDPN exposure leads to a predominantly type I HC loss, with only a slight decrease of type II HC at the highest dose, without additional functional impairment. The two main populations of vestibular HC can be divided by several molecular, histological and functional properties[20]. Type I hair cells connect to vestibular afferents via a calyx-shaped synapse, which supports both quantal transmission (glutamate release) and non-quantal transmission. The latter allows for rapid and precise signal transmission, making it especially effective in rapidly encoding head movements[21,22]. In contrast, type II hair cells transmit information exclusively through quantal transmission via a bouton-like synapse[23,24]. The IDPN-induced specific loss of type I hair cells and downstream associated pathways directly impaired the vestibulo-ocular reflexes, while type II cells remained largely unaffected in most cases, thus highlighting the pivotal role of type I HC, and putatively of non-quantal transmission, in the different vestibule-ocular reflexes.

This study also furthers our understanding of vestibular function decline associated with HC graded loss as e.g. in aging. The degeneration of both cochlear and vestibular hair cells with advancing age is well documented, correlating with occurrences of dizziness, impaired balance, and deficits in spatial orientation[24,25]. The decrease in vestibular responses (e.g. VOR[23]) observed with aging, is hypothesized to contribute to falls in the elderly[3], highlighting the importance of studying age-related vestibular decline. Previous research has shown that type I hair cells are more sensitive to aging and degenerate faster than type II cells[7]. Our observations mirror this pattern, as IDPN predominantly affects type I cells, rendering it a valuable model to examine the functional consequences associated with gradual loss of hair cell. To our knowledge, this is the first individual-based structure-function correlation between vestibular hair cells and specific vestibular function, filling a critical gap for the development of inner ear therapeutic treatments.

Recent advances in gene therapy, such as adeno-associated virus vectors[26], antisens oligonucleotides[27], or even lentiviral vectors[28], have shown promises in restoring hair cells and vestibular function. Our data provides important benchmarks for future therapies. Specifically, our results indicate that restoring at least 1/2 hair cell integrity appears mandatory to allow minimal vestibular function, while 3/4 of functional hair cells are required

263 for near-normal VOR responses. A targeted approach to specifically restore type I HC seems
264 mandatory to spare VORs function. Whether these thresholds are similar for other vestibular
265 functions (e.g., vestibulo-spinal reflexes and balance or vestibulo-thalamic pathways and
266 spatial orientation/perception) remains to be studied. In any case, these thresholds align with
267 recent gene therapy findings, where a significant otolithic hair cells regeneration could be
268 achieved in adult mice leading to a small functional restoration[10], while a recovery of less than
269 50% of hair cells did not improve vestibulo-ocular reflexes[12]. Hence, the current data support
270 the conclusion that future genetic-based interventions should achieve a threshold of
271 functional vestibular hair cells exceeding 50% to induce at least a minimal yet significant level
272 of vestibular recovery.
273 In summary, our research supports the importance of type I hair cells in vestibular function
274 and demonstrates that IDPN-induced hair cell loss is a valuable model for investigating
275 vestibular physiology and pathophysiology. Moreover, our findings emphasize key functional
276 thresholds for hair cell regeneration, providing a framework for the advancement of future
277 therapies targeting the restoration of vestibular function.
278
279 **Figure legends**
280 **Figure 1. Dose-dependent ototoxic effect on vestibulo-ocular reflexes**
281 A) Bode plot of the gain of the horizontal angular vestibulo-ocular reflex at different
282 frequencies (tested with sinusoidal rotations at peak velocity 30°/s) for the 5 different
283 concentration tested.
284 B) Maximal gain response in respond to abrupt horizontal acceleration/deceleration (steps of
285 acceleration from 0 to 50°/s, with peak velocity 250°/s²).
286 C) Gain of the ocular-counter roll reflex measured during static roll in range ±0-40.
287 D) Dynamic ocular-counter roll reflex gain. The gain was calculated using the vertical
288 component of the compensatory eye movement evoked in response to off-vertical axis
289 rotation with a tilt angle of 17°.
290 In all panels, sample sizes are: [Control] (n=7), [16] (n=8), [24] (n=8), [32] (n=7) and [40] (n=6).
291 Vertical and horizontal brackets indicate significant differences ($p<0.05$). Values represented
292 mean±SEM.
293
294 **Figure 2. Dose-dependent ototoxic effect on vestibular hair cells**

295 A) Immuno-labelling of all hair cells (Myo7a+), type I HC (Spp1+) and type II HC (Calre+) in the
296 central ampulla of the horizontal canal in SHAM [0] (left panels), and mice injected with [24]
297 (middle panels)] or [40] mmol/kg of IDPN. Samples were obtained at D21 following IDPN
298 injection.
299 (B, C, D) Cell count of hair cells in the central and peripheral horizontal ampulla for all IDPN
300 doses, with (B) Myo7a+ marker (all HC) (C) Spp1+ marker (type I specific marker), (D) Calre+
301 marker (type II specific). Sample size Sham (n=7), [16] (n=8), [24] (n=8), [32] (n=7) and [40]
302 (n=6).
303 E) Correlation matrix of the r Pearson coefficient of the number of HCI and HCII for the n=36
304 mice in different regions of ampulla and macula (Grey scheme; C.C: crista central, C.P: crista
305 periphery, M.C: macula central, M.M.P: macula medial periphery, M.L.P: macula lateral
306 periphery). The color code representing the values of the coefficient are in the top left panel.
307 F) Relation between number of type I HC in the macula and the number of type I HC in the
308 ampula in the central region of vestibular organs of individuals. The linear fit is represented.
309 G-H) Relation between number of type II HC in the ampulla and the number of type I HC in
310 the ampulla in the central (G) or peripheral (H) regions of individuals. The linear fit is
311 represented.
312
313 **Figure 3: Relation between hair cells subtype and vestibulo-ocular reflexes**
314 A,B,C,D) Normalized Mean aVOR (A), Hsteps (B), OCR (C) OCR Dyn (D), as a function of the
315 normalized number of Type I hair cells in the central part of the ampulla (A, B) or the central
316 part of the macula (C, D). The non-linear 2D fit is represented.
317 E,F,G,H) Normalized Mean aVOR (E), Hsteps (F), OCR (G) OCR Dyn (H), as a function of the
318 normalized number of Type II hair cells in the central part of the ampulla (E,F) or the central
319 part of the macula (G,H). The non-linear 2D fit is represented.
320 I,J,K,L) Error Fit (%) of the 2D sigmoid fit for the Mean aVOR (I), Hsteps (J), OCR (K) OCR Dyn
321 (L) in the central region and peripheral regions of the ampulla (I, J) or the macula (K, L) for
322 type I HC, type II HC and All Types (Type I + Type II).
323
324 **Figure 4: proportion of hair cells to maintain minimal and normal vestibular responses**

A) Number of type I hair cells counted in all regions of ampulla and macula (C.C: crista central, C.P: crista periphery, M.C: macula central, M.M.P: macula medial periphery, M.L.P: macula lateral periphery).

B) Clustering dendrogram of the individuals based on their number of type I hair cells in the different regions shown in (A).

C, D) Number of Myo7a-labelled hair cells as a function of the additive number of Spp1- and Calre-labelled hair cells in the ampulla (C) and macula (D).

E, F) Normalized Mean aVOR gain (E) and HSteps gain max (F) as a function of the normalized number of Myo7a-labelled hair cells in all regions of the ampulla.

G, H) Normalized static OCR gain (G) and Dynamical OCR gain (H) as a function of the normalized number of Myo7a-labelled hair cells in all regions of the macula.

In panel E-G the lowest (highest) threshold is obtained as the value of the sigmoidal fit, black line, for value of mean + (-) standard deviation of the pink (green) cluster group.

I) Superimposed 2D Non-linear fits of the vestibular hair cells integrity (%) as a function of the percentage of canal (black) and otolithic function (blue).

Supplementary Figure 1: Mean aVOR gain (A), HStep gain (B), static OCR gain (C), Dynamic OCR gain (D) of all (n=36) mice at D14 and D21 after injection.

Supplementary Figure 2: (A, B, C) Cell count of hair cells in the central and peripheral utricule for all IDPN doses, with (A) Myo7a+ marker (all HC) (B) Spp1+ marker (type I specific marker), (C) Calre+ marker (type II specific). Sample size Sham (n=7), [16] (n=8), [24] (n=8), [32] (n=7) and [40] (n=6).

Statistical Tables

Table 1 : Statistical tables for the 5 frequencies tested of the aVOR (Figure 1)

NaCl	16	24	32	40	0,2Hz
	ns	ns	***	***	NaCl
		ns	**	**	16
			ns	ns	24
				ns	32
					40

NaCl	16	24	32	40	0,5Hz
	ns	*	***	***	NaCl
		ns	**	***	16
			ns	ns	24
				ns	32
					40

NaCl	16	24	32	40	0,8Hz
	ns	*	***	***	NaCl
		ns	***	***	16
			ns	ns	24
				ns	32
					40

NaCl	16	24	32	40	1Hz
	ns	*	***	***	NaCl
		ns	***	***	16
			ns	ns	24
				*	32
					40

NaCl	16	24	32	40	2Hz
	ns	*	***	***	NaCl
		ns	***	***	16
			ns	*	24
				ns	32
					40

MATERIELS ET METHODS

ANIMALS

A total of 36 male and female C57/BL6J mice, age 6–10 weeks, was used in this study. Mice were kept in standard lighting and housing conditions. Animals were used in accordance with the European Communities Council Directive 2010/63/EU. All efforts were made to minimize suffering and reduce the number of animals included in the study. All procedures were approved by the ethical committee for animal research of the Université Paris Cité.

389 HEAD POST IMPLANTATION

390

391 Head post implantation surgery was performed as previously described[29]. Mice were
392 anesthetized with isoflurane, and a small longitudinal incision was made on their shaved head
393 to expose the skull after a local injection of lidocaine hydrochloride (2%; 2 mg/Kg). A custom-
394 built headpost 3×3×5mm; poly lactic acid) was first cemented (C&B Metabond; Parkell Inc.,
395 Edgewood, NY) and the sides were then covered with resin (Heraeus) for protection. Mice
396 were placed under red light post-surgery until their full recovery and were monitored for the
397 following 48h.

398

399 OTOTOXIC EXPOSURE

400

401 Mice were treated with a single IP injection of IDPN. The animals were divided into 5 groups
402 that received different doses of IDPN: 16 mmol/kg (n=8), 24 mmol/kg (n=8), 32 mmol/kg
403 (n=7), 40 (n=6) mmol/kg and the control group (n=7) that received an injection of NaCl.
404 Vestibular function was tested 2 (D14) and 3 weeks (D21) after the injection. As the longer
405 time after exposure led to no further vestibular function deprivation (mix-model statistical
406 test, non-significant differences between D14 and D21 for each test (aVOR, Hsteps, OCR and
407 OCR Dynamic, see supplementary Figure 1), D14 and D21 functional data were pooled.

408

409 VIDEO OCULOGRAPHY RECORDING SESSIONS

410

411 Eye movements were recorded with a non-invasive video-oculography system (ETL 200 Iscan,
412 Acquisition rate 120 Hz) following procedure previously described[30]. In brief, mice were
413 positioned in a Plexigas tube and head-fixed with a nose-down angle of 30° to align the
414 horizontal semi-circular canals with the yaw plane. The tube was fixed on a rotating platform
415 on top of an extended rig with a servo-controlled motor. Eye and Image/head position signals
416 were sampled at 1 kHz, digitally recorded (CED power1401 MkII) with Spike 2 software and
417 analyzed off-line in Matlab (Matlab, The MathWorks, Natick, MA, USA; RRID: SCR:001622)
418 programming environment. Recording sessions were performed in a temperature-controlled
419 room (21-24°) and lasted up to 45 min.

420

VESTIBULAR STIMULATION

Canal (VORd and Hsteps) and utricular-specific (OCR and OCR Dynamic) tests were performed in complete darkness, with the mouse surrounded by an opaque dome or box. Pilocarpine 2% was placed on the eye of the mouse before the test to prevent excessive pupil dilatation.
Sinusoidal angular rotations around the vertical axis were performed to record the horizontal angular vestibulo-ocular reflex (aVOR), at different frequencies: 0.2, 0.5, 0.8; 1 and 2Hz at a peak velocity of 30°/s. At least 10 cycles were analysed per frequency and the compensatory eye movements were quantified by calculating the gain (ratio between the eye velocity and table velocity) and the phase (normalized latency between the eye and the table velocities)[31].
HSteps test were performed using an abrupt acceleration followed by a sudden stop after three 360° rotations with a constant-velocity of 50°/s on the yaw plane (acceleration 250°/s²). The hsteps gain was calculated as the ratio between the peak velocity of the slow phases at onset and offset of rotations, and the rotation velocity.
Static Counter Roll (OCR) tests were performed first by measuring the vertical pupil position according to the head tilt angle at 0° in the horizontal plane. The table was then tilted from left to right in incremental steps of 10° (from 0 to 40deg), with static periods of at least 10s between oscillations (Fig1.D) to record stable eye position. The OCR gain corresponds to the slope of the linear regression of the vertical eye angle and the head tilt angles[32,31].
Dynamic OCR tests were performed with the vestibular turntable tilted with a 17° off-axis angle[16,34,35]. 50°/s continuous stimulations were performed in a counter-clockwise and then clockwise direction. The Dynamic OCR gain corresponds to the dynamic, or vertical component of the compensatory eye movement divided by the maximal differential tilt angle (i.e 34°).

IMMUNOLABELLING OF THE HAIR CELLS IN THE HORIZONTAL SEMI-CIRCULAR CANALS AND THE UTRICULE

The inner ear of all mice tested with vestibular function tests (n=36) were then used to perform immunofluorescence analysis on hair cells in the vestibular endorgans. Mice were anaesthetized with an overdose of intraperitoneal injection of ketamine hydrochloride (10%)/xylazine (5%) and decapitated. The histology was done following previously published

protocol of Maroto and colleagues[9]. The vestibular epithelia were dissected and fixed for 1h in a 4% solution of paraformaldehyde (PFA). PFA was washed twice with phosphate-buffered saline (PBS) and the samples were placed in a cryoprotective solution at 4° for 2h for effective embedding and then stored at -20°. Before the immunochemistry, samples (one horizontal canal and one utricule) were put at room temperature and rinsed twice in PBS. While under slow agitation, the samples were incubated twice, first for 1h with 4% Triton X-100 (Sigma Aldrich) in PBS to permeabilise the tissue and a second time for 1h in 0.5% Triton X-100 1% fish gelatin (CAS #9000-70-8, Sigma-Aldrich) in PBS to block non-specific binding sites. The incubation with the primary antibodies was then performed in 0.1% Triton X-100, 1% fish gelatin in PBS at 4° for 24h. After rinsing, the secondary antibodies were incubated in the same conditions. The secondary antibodies were rinsed and the vestibular epithelia were mounted on slides with fluoromount (F4680, Sigma-Aldrich) and were visualised with a Zeiss LSM880 confocal microscope (with an objective of 63x NA:1;4). To properly analyse the whole vestibular epithelium, Z-stacks of 0.5 µm were obtained and observed with ImageJ (National Institute of Mental Health, Bethesda, Malyland, USA). The primary antibodies used were rabbit anti-Myosin VIIa (Myo7a) (Proteus Biosciences, #25-6790, 1:400), guinea pig anti calretinin (Synaptic Systems #214-104, 1:500) and goat anti-osteopontin (SPP1) (R&D Systems #AF08, 1:200). Their respective secondary antibodies were Dylight 405 donkey anti-rabbit ifG H+L (Jackson Immuno Research #711-475-152, Alexa Fluor 488 donkey anti-guinea-pig IgG H+L (Jackson ImmunoResearch #706-605-148) and Alexa Fluor 555 donkey anti-goat IgG H+L (Invitrogen #A21432).

The global number of hair cells was assessed with the cytoplasmic labelling of the anti-Myo7a antibody[36]. Type I hair cells were labelled using anti-SPP1, found in the neck of the type I HC[37]. Type II hair cells were distinguished by the colocalization of Myo7a and calretinin[38]. A thorough evaluation of the specificity of these markers in the adult rat has been recently published[17].

STATISTICAL ANALYSIS

To test the main effect of the between-individual factor 'Dose' (0, 16, 24, 32 or 40 mmol/kg) on Hsteps, OCR and DYN OCR, as well as the effect of IDPN exposure on the hair cells, a one-way ANOVA was used. For the aVOR a two-ways ANOVA was used to be able to evaluate also

485 the main effect of the within-individual independent factor 'Frequency' (0.2, 0.5, 0.8, 1 and
486 2Hz) and its interaction with the Dose. The difference between D14 and D21 vestibular reflex
487 tests was reported with a mixed model analysis. The significance threshold was set at $p<0.05$
488 and Tukey multiple comparison test was performed if the main effect, or an interaction, was
489 reported significant.
490 To describe the relationship between cell staining and the behavioural measures, 2D non-
491 linear (sigmoidal) models were used to fit the datasets. Given the presence of noise on both
492 types of measurement (function and cell counting data), the fitting required orthogonal
493 distance regression and the fit was optimized for each data set.
494
495 BIBLIOGRAPHY
496

497 1. Emptoz, A., Michel, V., Lelli, A., Akil, O., Boutet De Monvel, J., Lahlou, G., Meyer, A.,
498 Dupont, T., Nouaille, S., Ey, E., et al. (2017). Local gene therapy durably restores
499 vestibular function in a mouse model of Usher syndrome type 1G. Proc. Natl. Acad. Sci.
500 U.S.A. *114*, 9695–9700. https://doi.org/10.1073/pnas.1708894114.

501 2. Agrawal, Y., Ward, B.K., and Minor, L.B. (2013). Vestibular dysfunction: Prevalence,
502 impact and need for targeted treatment. VES *23*, 113–117. https://doi.org/10.3233/VES-
503 130498.

504 3. Maudoux, A., Vitry, S., and El-Amraoui, A. (2022). Vestibular Deficits in Deafness: Clinical
505 Presentation, Animal Modeling, and Treatment Solutions. Front. Neurol. *13*, 816534.
506 https://doi.org/10.3389/fneur.2022.816534.

507 4. Paplou, V., Schubert, N.M.A., and Pyott, S.J. (2021). Age-Related Changes in the Cochlea
508 and Vestibule: Shared Patterns and Processes. Front. Neurosci. *15*, 680856.
509 https://doi.org/10.3389/fnins.2021.680856.

510 5. Walther, L.E., and Westhofen, M. (2008). Presbyvertigo-aging of otoconia and vestibular
511 sensory cells. VES *17*, 89–92. https://doi.org/10.3233/VES-2007-172-303.

512 6. Merchant, S.N., Tsuji, K., and Wall, C. Temporal Bone Studies of the Human Peripheral
513 Vestibular System.

514 7. Rauch, S.D., Velazquez-Villaseñor, L., Dimitri, P.S., and Merchant, S.N. (2001). Decreasing
515 Hair Cell Counts in Aging Humans. Annals of the New York Academy of Sciences *942*,
516 220–227. https://doi.org/10.1111/j.1749-6632.2001.tb03748.x.

517 8. Lopez, I., Ishiyama, G., Tang, Y., Tokita, J., Baloh, R.W., and Ishiyama, A. (2005). Regional
518 estimates of hair cells and supporting cells in the human crista ampullaris. J. Neurosci.
519 Res. *82*, 421–431. https://doi.org/10.1002/jnr.20652.

9. Maroto, A.F., Barrallo-Gimeno, A., and Llorens, J. (2021). Relationship between vestibular hair cell loss and deficits in two anti-gravity reflexes in the rat. Hearing Research *410*, 108336. https://doi.org/10.1016/j.heares.2021.108336.

10. Lahlou, H., Zhu, H., Zhou, W., and Edge, A.S.B. (2024). Pharmacological regeneration of sensory hair cells restores afferent innervation and vestibular function. Journal of Clinical Investigation. https://doi.org/10.1172/JCI181201.

11. Lahlou, G., Calvet, C., Simon, F., Michel, V., Alciato, L., Plion, B., Boutet De Monvel, J., Lecomte, M.-J., Beraneck, M., Petit, C., et al. (2024). Extended time frame for restoring inner ear function through gene therapy in Usher1G preclinical model. JCI Insight *9*, 1–14. https://doi.org/10.1172/jci.insight.169504.

12. Jáuregui, E., Scheinman, K., BibriescaMejia, I., Finkbeiner, C., Phillips, J.A., Gantz, J.A., Phillips, J., and Stone, J. (2024). Sensorineural correlates of failed functional recovery after natural regeneration of vestibular hair cells in adult mice. Front. Neurol. https://doi.org/10.3389/fneur.2024.1322647.

13. Schenberg, L., Palou, A., Simon, F., Bonnard, T., Barton, C.-E., Fricker, D., Tagliabue, M., Llorens, J., and Beraneck, M. (2023). Multisensory gaze stabilization in response to subchronic alteration of vestibular type I hair cells. eLife *12*, RP88819. https://doi.org/10.7554/eLife.88819.

14. Soler-Martin, C., Diez-Padrisa, N., Boadas-Vaello, P., and Llorens, J. (2006). Behavioral Disturbances and Hair Cell Loss in the Inner Ear Following Nitrile Exposure in Mice, Guinea Pigs, and Frogs. Toxicological Sciences *96*, 123–132. https://doi.org/10.1093/toxsci/kfl186.

15. Llorens, J., Demêmes, D., and Sans, A. (1993). The behavioural syndrome caused by 3’3-Iminodipropionitrile and related nitriles in the rat is associated with degeneration of the vestibular sensory hair cells. Toxicology and Applied Pharmacology, 199–210.

16. Beraneck, M., Bojados, M., Le Séac’h, A., Jamon, M., and Vidal, P.-P. (2012). Ontogeny of Mouse Vestibulo-Ocular Reflex Following Genetic or Environmental Alteration of Gravity Sensing. PLoS ONE *7*, e40414. https://doi.org/10.1371/journal.pone.0040414.

17. Borrajo, M., Sedano, D., Palou, A., Giménez-Esbrí, V., Barrallo-Gimeno, A., and Llorens, J. (2024). Maturation of type I and type II rat vestibular hair cells in vivo and in vitro. Front. Cell Dev. Biol. *12*, 1404894. https://doi.org/10.3389/fcell.2024.1404894.

18. Martins-Lopes, V., Bellmunt, A., Greguske, E.A., Maroto, A.F., Boadas-Vaello, P., and Llorens, J. (2019). Quantitative Assessment of Anti-Gravity Reflexes to EvaluateVestibular Dysfunction in Rats. JARO *20*, 553–563. https://doi.org/10.1007/s10162-019-00730-6.

19. Zeng, S., Ni, W., Jiang, H., You, D., Wang, J., Lu, X., Liu, L., Yu, H., Wu, J., Chen, F., et al. (2020). Toxic Effects of 3,3 ’ -Iminodipropionitrile on Vestibular System in Adult C57BL/6J Mice *In Vivo*. Neural Plasticity *2020*, 1–11. https://doi.org/10.1155/2020/1823454.

20. Eatock, R.A., and Songer, J.E. (2011). Vestibular Hair Cells and Afferents: Two Channels for Head Motion Signals. Annu. Rev. Neurosci. *34*, 501–534. https://doi.org/10.1146/annurev-neuro-061010-113710.

21. Spaiardi, P., Marcotti, W., Masetto, S., and Johnson, S.L. (2022). Signal transmission in mature mammalian vestibular hair cells. Front. Cell. Neurosci. *16*, 806913. https://doi.org/10.3389/fncel.2022.806913.

22. Govindaraju, A.C., Quraishi, I.H., Lysakowski, A., Eatock, R.A., and Raphael, R.M. (2023). Nonquantal transmission at the vestibular hair cell–calyx synapse: K_{LV} currents modulate fast electrical and slow K^+ potentials. Proc. Natl. Acad. Sci. U.S.A. *120*, e2207466120. https://doi.org/10.1073/pnas.2207466120.

23. Songer, J.E., and Eatock, R.A. (2013). Tuning and Timing in Mammalian Type I Hair Cells and Calyceal Synapses. Journal of Neuroscience *33*, 3706–3724. https://doi.org/10.1523/JNEUROSCI.4067-12.2013.

24. Contini, D., Holstein, G.R., and Art, J.J. (2022). Simultaneous Dual Recordings From Vestibular Hair Cells and Their Calyx Afferents Demonstrate Multiple Modes of Transmission at These Specialized Endings. Front. Neurol. *13*, 891536. https://doi.org/10.3389/fneur.2022.891536.

25. Burns, J.C., and Stone, J.S. (2017). Development and regeneration of vestibular hair cells in mammals. Seminars in Cell & Developmental Biology *65*, 96–105. https://doi.org/10.1016/j.semcdb.2016.11.001.

26. Isgrig, K., Shteamer, J.W., Belyantseva, I.A., Drummond, M.C., Fitzgerald, T.S., Vijayakumar, S., Jones, S.M., Griffith, A.J., Friedman, T.B., Cunningham, L.L., et al. (2017). Gene Therapy Restores Balance and Auditory Functions in a Mouse Model of Usher Syndrome. Molecular Therapy *25*, 780–791. https://doi.org/10.1016/j.ymthe.2017.01.007.

27. Lentz, J.J., Jodelka, F.M., Hinrich, A.J., McCaffrey, K.E., Farris, H.E., Spalitta, M.J., Bazan, N.G., Duelli, D.M., Rigo, F., and Hastings, M.L. (2013). Rescue of hearing and vestibular function by antisense oligonucleotides in a mouse model of human deafness. Nat Med *19*, 345–350. https://doi.org/10.1038/nm.3106.

28. Schott, J.W., Huang, P., Morgan, M., Nelson-Brantley, J., Koehler, A., Renslo, B., Büning, H., Warnecke, A., Schambach, A., and Staecker, H. (2023). Third-generation lentiviral gene therapy rescues function in a mouse model of Usher 1B. Molecular Therapy *31*, 3502–3519. https://doi.org/10.1016/j.ymthe.2023.10.018.

29. França de Barros, F., Schenberg, L., Tagliabue, M., and Beraneck, M. (2020). Long term visuo-vestibular mismatch in freely behaving mice differentially affects gaze stabilizing reflexes. Sci Rep *10*, 20018. https://doi.org/10.1038/s41598-020-77026-w.

30. Stahl, J.S. (2004). Using eye movements to assess brain function in mice. Vision Research *44*, 3401–3410. https://doi.org/10.1016/j.visres.2004.09.011.

31. Carcaud, J., França de Barros, F., Idoux, E., Eugène, D., Reveret, L., Moore, L.E., Vidal, P.-P., and Beraneck, M. (2017). Long-Lasting Visuo-Vestibular Mismatch in Freely-Behaving Mice Reduces the Vestibulo-Ocular Reflex and Leads to Neural Changes in the Direct Vestibular Pathway. eNeuro *4*, ENEURO.0290-16.2017. https://doi.org/10.1523/ENEURO.0290-16.2017.

32. Oommen, B.S., and Stahl, J.S. (2008). Eye orientation during static tilts and its relationship to spontaneous head pitch in the laboratory mouse. Brain Research *1193*, 57–66. https://doi.org/10.1016/j.brainres.2007.11.053.

33. Simon, F., Pericat, D., Djian, C., Fricker, D., Denoyelle, F., and Beraneck, M. (2020). Surgical techniques and functional evaluation for vestibular lesions in the mouse: unilateral labyrinthectomy (UL) and unilateral vestibular neurectomy (UVN). J Neurol *267*, 51–61. https://doi.org/10.1007/s00415-020-09960-8.

34. Idoux, E., Tagliabue, M., and Beraneck, M. (2018). No Gain No Pain: Relations Between Vestibulo-Ocular Reflexes and Motion Sickness in Mice. Front. Neurol. *9*, 918. https://doi.org/10.3389/fneur.2018.00918.

35. Simon, F., Tissir, F., Michel, V., Lahlou, G., Deans, M., and Beraneck, M. (2021). Implication of Vestibular Hair Cell Loss of Planar Polarity for the Canal and Otolith-Dependent Vestibulo-Ocular Reflexes in Celsr1–/– Mice. Front. Neurosci. *15*, 750596. https://doi.org/10.3389/fnins.2021.750596.

36. Hasson, T., Gillespie, P.G., Garcia, J.A., MacDonald, R.B., Zhao, Y., Yee, A.G., Mooseker, M.S., and Corey, D.P. (1997). Unconventional Myosins in Inner-Ear Sensory Epithelia. Journal of Cell Biology *137*, 1287–1307. https://doi.org/10.1083/jcb.137.6.1287.

37. McInturff, S., Burns, J.C., and Kelley, M.W. (2018). Characterization of spatial and temporal development of Type I and Type II hair cells in the mouse utricle using new cell-type-specific markers. Biology Open *7*, bio038083. https://doi.org/10.1242/bio.038083.

38. Dechesne, C.J., Winsky, L., Kim, H.N., Goping, G., Vu, T.D., Wenthold, R.J., and Jacobowitz, D.M. (1991). Identification and ultrastructural localization of a calretinin-like calcium-binding protein (protein 10) in the guinea pig and rat inner ear. Brain Research *560*, 139–148. https://doi.org/10.1016/0006-8993(91)91224-O.

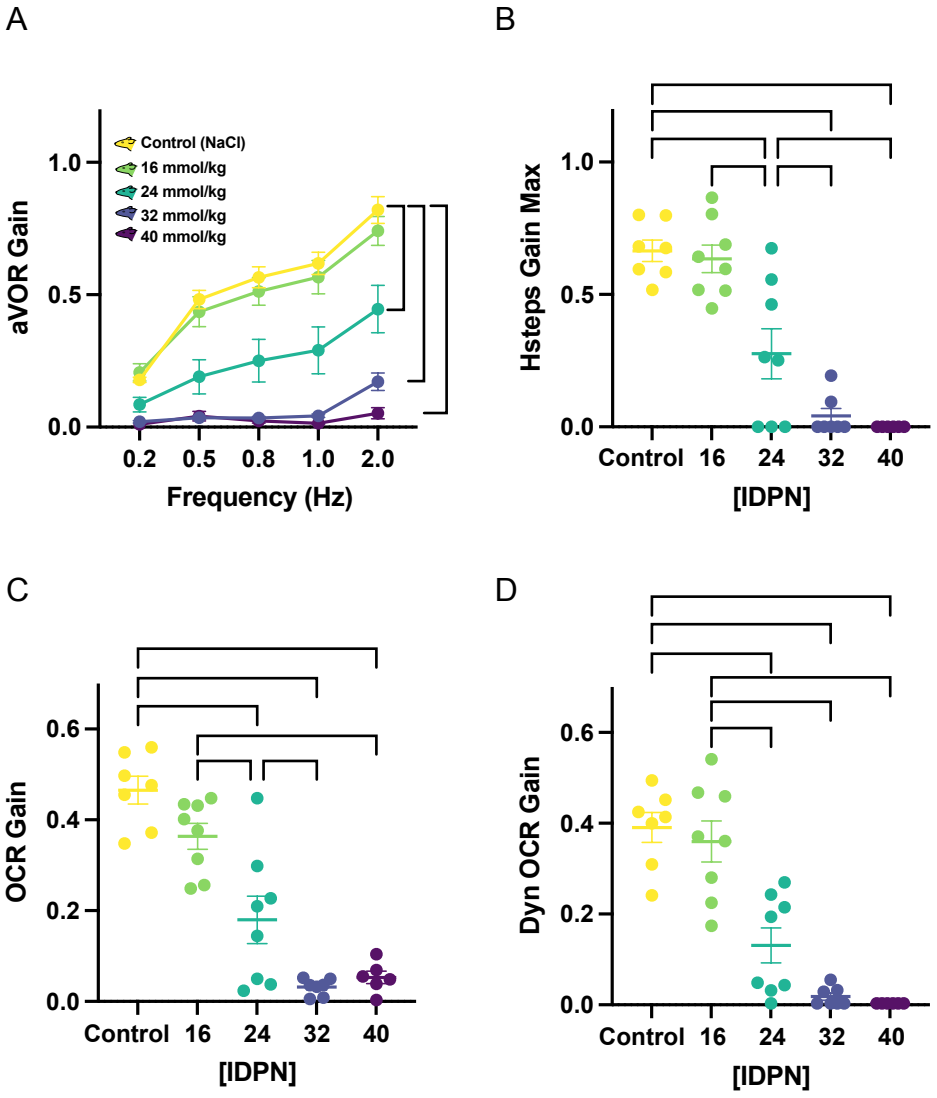
A
Control (NaCl)
16 mmol/kg
24 mmol/kg
32 mmol/kg
40 mmol/kg
aVOR Gain
1.0
0.5
0.0
0.2
0.5
0.8
1.0
2.0
Frequency (Hz)
B
Hsteps Gain Max
1.0
0.5
0.0
Control
16
24
32
40
[IDPN]
C
OCR Gain
0.6
0.4
0.2
0.0
Control
16
24
32
40
[IDPN]
D
Dyn OCR Gain
0.6
0.4
0.2
0.0
Control
16
24
32
40
[IDPN]

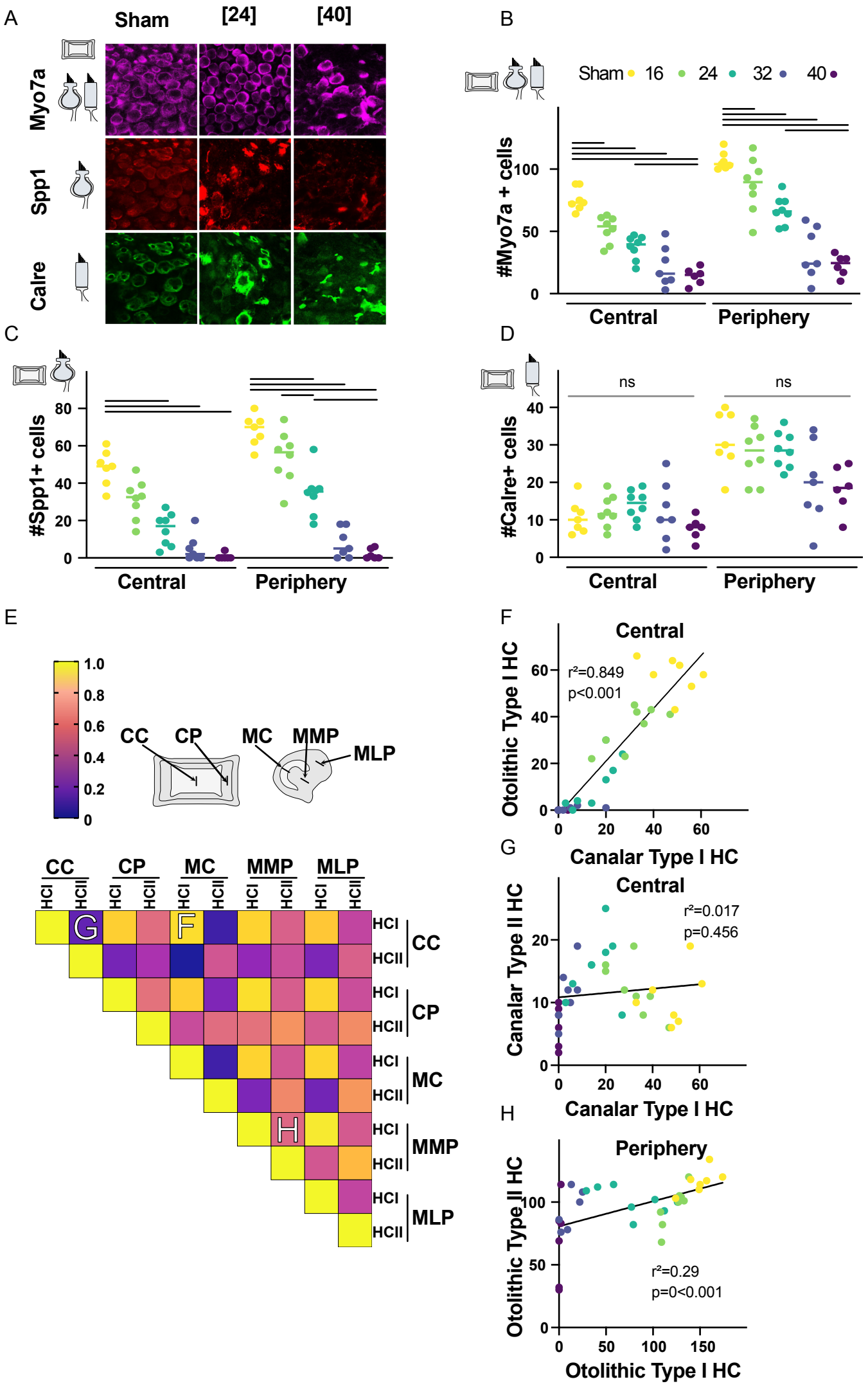
A
Sham
[24]
[40]
Myo7a
Spp1
Calre
B
Sham 16 24 32 40
#Myo7a + cells
Central
Periphery
C
#Spp1+ cells
Central
Periphery
D
ns
ns
#Calre+ cells
Central
Periphery
E
1.0
0.8
0.6
0.4
0.2
0
CC
CP
MC
MMP
MLP
HCI
HCII
F
Central
r²=0.849
p<0.001
Otolithic Type I HC
Canalar Type I HC
G
Central
r²=0.017
p=0.456
Canalar Type II HC
Canalar Type I HC
H
Periphery
r²=0.29
p=0<0.001
Otolithic Type II HC
Otolithic Type I HC

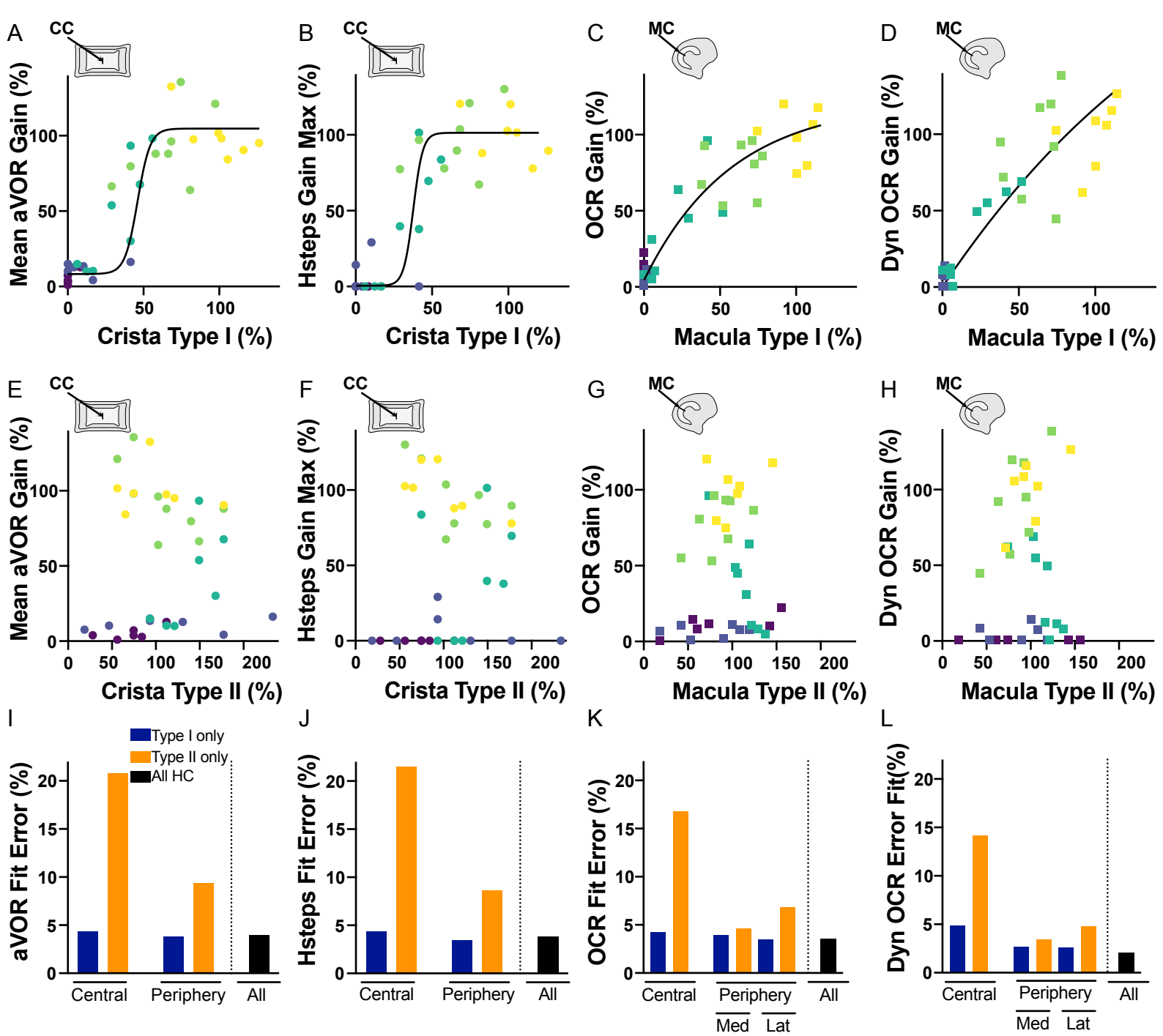
A
CC
Mean aVOR Gain (%)
Crista Type I (%)
B
CC
Hsteps Gain Max (%)
Crista Type I (%)
C
MC
OCR Gain (%)
Macula Type I (%)
D
MC
Dyn OCR Gain (%)
Macula Type I (%)
E
CC
Mean aVOR Gain (%)
Crista Type II (%)
F
CC
Hsteps Gain Max (%)
Crista Type II (%)
G
MC
OCR Gain (%)
Macula Type II (%)
H
MC
Dyn OCR Gain (%)
Macula Type II (%)
I
Type I only
Type II only
All HC
aVOR Fit Error (%)
Central
Periphery
All
J
Hsteps Fit Error (%)
Central
Periphery
All
K
OCR Fit Error (%)
Central
Periphery
Med
Lat
All
L
Dyn OCR Error Fit(%)
Central
Periphery
Med
Lat
All

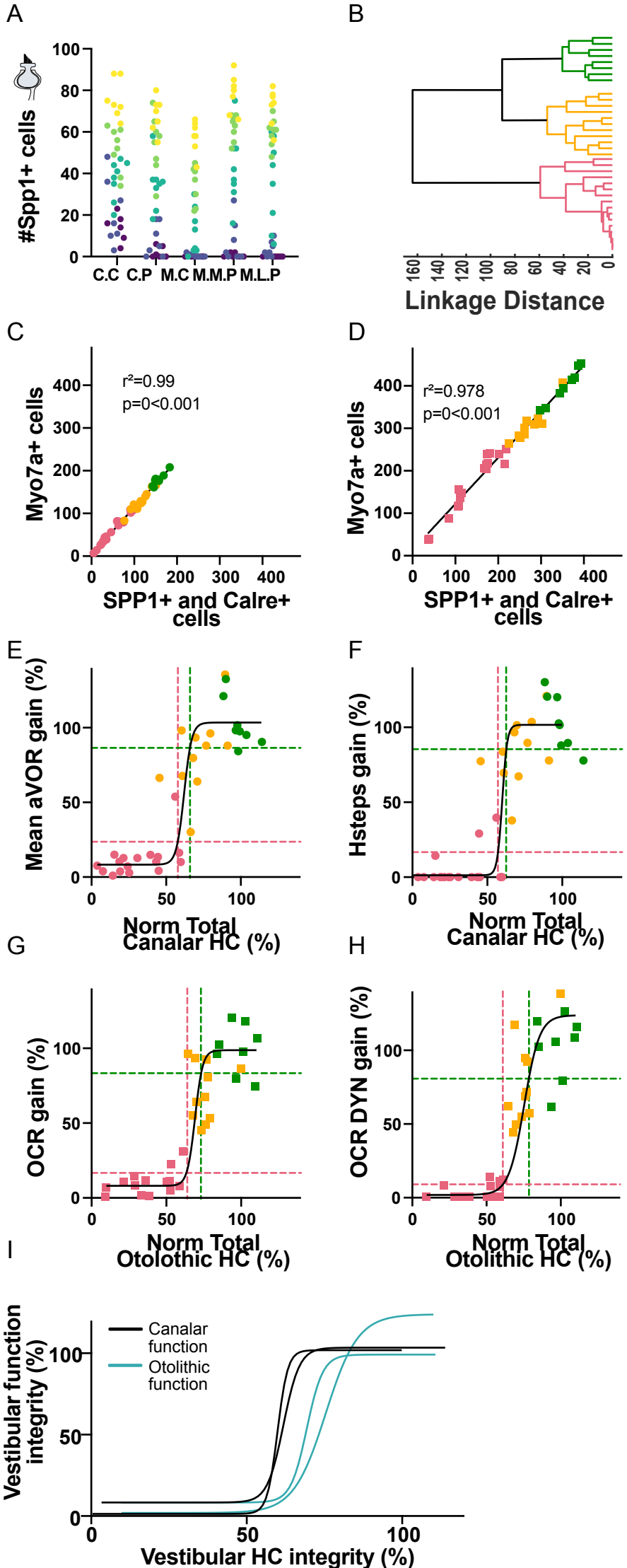
A
#Spp1+ cells
C.C
C.P
M.C
M.M.P
M.L.P
B
Linkage Distance
C
Myo7a+ cells
r²=0.99
p=0<0.001
SPP1+ and Calre+ cells
D
Myo7a+ cells
r²=0.978
p=0<0.001
SPP1+ and Calre+ cells
E
Mean aVOR gain (%)
Norm Total Canalar HC (%)
F
Hsteps gain (%)
Norm Total Canalar HC (%)
G
OCR gain (%)
Norm Total Otolothic HC (%)
H
OCR DYN gain (%)
Norm Total Otolithic HC (%)
I
Vestibular function integrity (%)
Canalar function
Otolithic function
Vestibular HC integrity (%)